Behavior of microbubbles in homogeneous stratified turbulence

Gihun Shim [ORCID][*] and Hyeongjun Park
Department of Computational Science & Engineering, Yonsei University, Seoul, 03722, Korea

Seulgi Lee
Department of Mechanical Engineering, Yonsei University, Seoul, 03722, Korea

Changhoon Lee[†]
Department of Computational Science & Engineering, Yonsei University, Seoul, 03722, Korea
and Department of Mechanical Engineering, Yonsei University, Seoul, 03722, Korea

Dynamic behaviors of spherical microbubbles, within a one-way coupling frame, in stratified turbulence are investigated by direct numerical simulation. To simulate stratified turbulence, the Navier-Stokes equations and heat equation with a background linear temperature variation are solved in a periodic cube domain. Stratification creates a predominantly horizontal motion in a fluid, thereby inducing the well-defined "quasi" mean oscillatory horizontal flow. By solving the equation of motion for microbubbles, we found that the clustering of bubbles with a Stokes number below 0.1 becomes weaker as the stratification is increased. Consequently, the reduction of rise velocity of bubbles in turbulence compared to that in still fluid decreases from 7% to 2%. Owing to the alternating mean motion of the fluid, bubbles rise in a zigzag pattern, thereby resulting in an oscillatory Lagrangian correlation of the horizontal velocity component of bubbles. Despite this oscillating rising motion of the bubbles, the horizontal dispersion of a single bubble is suppressed. From the statistics of the horizontal separation of pair bubbles, we observe a power-law growth in the Batchelor and Richardson regimes for the separation.

I. INTRODUCTION

Interactions between particles and stratified turbulence are frequently observed in nature, such as with small dust particles in the atmosphere, fine bubbles and phytoplankton in the oceans, and sediment transport in rivers. It also can be found in industry, such as in fluidized bed reactors, combustion engines, and atomic piles (see recent reviews [1,2]). The dynamics of particles in a stratified environment are clearly different from those in a nonstratified environment and this difference plays a critical role in the behavior of these particles. In oceanic turbulence, for instance, the motion of noninertial marine particles is determined by the interaction between these particles and stratified turbulence. Yamazaki *et al.* [3] examined the planktonic contact rates in stratified oceanic turbulence by direct numerical simulation. They compared the contact rates under two circumstances, with turbulence and in stagnant fluid, and determined that the contact rates generally increase with turbulence. Rothschild and Osborn [4] proved the theory that an increase in turbulent fluctuations enhances the contact rates of phytoplankton. Marrase *et al.* [5] conducted experiments

---

[*]lingenious2@gmail.com
[†]clee@yonsei.ac.kr

to investigate the effects of turbulence on encounter rates between copepods and their food, which also showed that the rates were higher in the presence of turbulence. Mixing efficiency of microorganisms in stratified flows at either low or intermediate Reynolds number was also investigated, showing that mixing in the vertical direction was predominant [6,7]. Overall trends between turbulence and marine organisms were well addressed in the above papers.

Stratified turbulence without any laden particles has been widely studied. Gerz and Yamazaki [8] investigated correlations between turbulent fluctuations and temperature perturbations by direct numerical simulation (DNS). Using a similar numerical method, Kimura and Herring [9] showed that the vertical diffusion of a pair of fluid particles decreases during strengthening stratification. Kaltenbach *et al.* [10] used large-eddy simulation (LES) and compared with DNS results, which were in good agreement with each other as the stratification remained weak. Turbulent mixing in terms of its efficiency has been described in detail in Refs. [11,12]. Peltier and Caulfield [11] asserted that mixing efficiency depends on the initial Richardson number, but did not show any definite proportional connections. Gonzalez-Juez *et al.* [12] reported that the vertical diffusivity was reciprocally proportional to the square of buoyancy frequency in intermediate *Re* regimes. The evolution of layer structures with turbulence was scrutinized in terms of various Richardson numbers, and those layers were determined to be formed by instability of local mixing [13–15]. The energy state at several resolutions was discussed in Ref. [16] via the horizontal energy spectra, which shows a -2 slope in the inertial subrange at the higher resolution. Refreshingly, scaling analysis was performed considering distinctive and nondimensional parameters to calculate the fluid properties of stratified turbulence with a reinterpretation [17,18]. Recently, Chung and Matheou [19] suggested investigation of turbulent statistics by subtracting those of mean flow based on Ref. [20]. They applied the framework of Monin–Obukhov similarity to homogeneous stratified turbulence to explain the vertical diapycnal diffusivity.

The dynamics of inertial particles in stratified turbulence have been investigated in recent years. Single-particle dispersion in horizontal and vertical directions was investigated in [21–23]. As time elapsed, particles with large Stokes numbers moved far away from their initial positions. Preferential clustering of heavy particles, depending on the Stokes number and vortical structure of the fluid, has also been studied [24–26]. Because an equation of motion of inertial particles commonly comprises components of drag forces and gravity, their behavior can be relatively easily described [21,23,24]. In contrast, spherical microbubbles show convoluted motions due to a combination of fluid acceleration with added effects due to mass, drag forces, buoyancy, and lift [27–29]. The dynamics of bubbles in isotropic turbulence have long been investigated in both numerical simulations and experiments. For instance, DNS with microbubbles, without consideration of a lift force, has been performed, reporting that bubbles accumulate in high-vorticity regions [30,31]. Taking into account the lift force, what causes the bubbles to push to the regimes of downwelling flows was analyzed by the motion of microbubbles using both DNS [27,28,32] and experiments [33,34]. To investigate bubble locomotion, several types of studies have been conducted. Through numerical and experimental studies, Mathai *et al.* [35] claimed that acceleration of small bubbles deviates from that of a fluid tracer because of the impact of turbulent flows. Alméras *et al.* [36] showed the variation of turbulent fluctuations induced from bubbles experimentally and successfully classified the fluctuation regimes as increasing or decreasing with a related parameter. Single and pair-wise dispersions of particles, starting with fluid pairs as the origin [37,38], were also analyzed. Bourgoin *et al.* [37] and Bourgoin [38] observed growing distances between fluid pairs with the scales of Batchelor and Richardson, and those scales seemed to be effective to describe the dispersion of bubbles. Mathai *et al.* [39] showed that the mean-square dispersion of single bubbles follows ballistic and diffusive regimes in order, regardless of the magnitude of the Taylor-scale Reynolds number. Recently, Kim *et al.* [40] reported pair-wise dispersion of bubbles in Rayleigh-Bérnald convection by varying the initial distances between them, finding that diffusivity is proportional to the initial distance. Despite numerous studies regarding bubbles in various types of turbulence, behaviors of bubbles in stratified turbulence have not yet been examined. Therefore, it is worthwhile to study the dynamic characteristics of bubbles in stratified turbulence through a

direct numerical simulation given that bubble-laden stratified turbulence is frequently observed, as discussed above.

In this study, we demonstrate the effects of stratified turbulence on the dynamics of microbubbles in a one-way coupling where the bubbles do not back-react on the flow, which is valid only for a low volume fraction. Prior to describing the behaviors of the bubbles, stratified turbulence is briefly discussed by noticing that there exists a "quasi" mean horizontal motion of the fluid. To identify the behavior of bubbles, the clustering nature of the bubbles and variations in their rise velocity are examined with different strengths of stratification. The horizontal motion of the bubbles is investigated in detail using various statistical methods, such as the Lagrangian bubble velocity correlation, single bubble dispersion and separation of a pair of bubbles.

The paper is organized as follows. In Sec. II, we describe the various attributes of the stratified turbulence and a comparison with isotropic turbulence using a direct numerical simulation. Next, the dynamic behaviors of microbubbles are analyzed in Sec. III. Finally, an overall summary of the simulation results is outlined in Sec. IV.

II. DESCRIPTION OF STRATIFIED TURBULENCE USING DIRECT NUMERICAL SIMULATION

Analyzing stratified turbulence is essential for studying the interaction between marine organisms and background turbulence in ocean thermoclines. The role of gases in the ocean is of primary interest in studies such as air-sea exchange of oxygen for marine organisms [41,42] and diapycnal mixing [43,44]. Although many attempts have been made to investigate stratified turbulence, only a few studies have been carried out that separate stratified turbulence into mean flows and turbulence. Chung and Matheou [19] utilized this approach, but did not focus on the characteristics of mean flows. Therefore, to understand the effects on collective structures of stratified turbulence effectively, we explore features of the mean flows and turbulent statistics, based on an approach similar to that of Ref. [19].

To numerically establish stratified turbulence, we solve the Navier-Stokes equations under the Boussinesq approximation, the heat equation, and the continuity equation with a background temperature $T_b(z)$, as described below:

$$\frac{\partial \boldsymbol{u}}{\partial t} + (\boldsymbol{u} \cdot \nabla)\boldsymbol{u} = -\frac{1}{\rho}\nabla P + \nu\nabla^2\boldsymbol{u} + \beta\boldsymbol{g}T' + \boldsymbol{f}, \tag{1}$$

$$\frac{\partial T'}{\partial t} + (\boldsymbol{u} \cdot \nabla)T' + \gamma u_z = \alpha\nabla^2 T', \tag{2}$$

$$\nabla \cdot \boldsymbol{u} = 0, \tag{3}$$

where $\boldsymbol{u}$, ρ, P, ν, α, β, $\boldsymbol{g}$, T', and $\boldsymbol{f}$ denote the fluid velocity, fluid density, modified pressure, kinematic viscosity, thermal diffusivity, volumetric expansion coefficient, gravitational acceleration vector acting in the $-z$ direction, temperature fluctuation, and large-scale force required to maintain the turbulence, respectively. u_z and $\gamma(= dT_b/dz)$ are the vertical component of fluid velocity and constant background temperature gradient, respectively [8]. Notably, the temperature $T(\boldsymbol{x}, t)$ and pressure p can be recovered by $T(\boldsymbol{x}, t) = T_b(z) + T'(\boldsymbol{x}, t)$, $p = P + \frac{\rho g \beta}{2}\gamma z^2$. To describe the characteristics of stratified turbulence, we introduce the following three nondimensional parameters: Taylor-scale Reynolds number, Re_λ, Froude number, Fr, and Prandtl number Pr, as defined below:

$$\mathrm{Re}_\lambda = \frac{u_{\mathrm{rms}}\lambda}{\nu}, \quad \mathrm{Fr} = \frac{u_{\mathrm{rms}}}{N\lambda}, \quad \mathrm{Pr} = \frac{\nu}{\alpha}, \tag{4}$$

where u_{rms}, λ, $N(= \sqrt{\beta g \gamma})$ are the root-mean-squared velocity, Taylor length scale of turbulence, and Brunt Väisälä frequency (or buoyancy frequency), respectively. The Froude number is smaller than 3.5 in typical real ocean thermoclines [3]. The Prandtl number is kept constant (Pr = 7) for water. Table I details information on the fluid and simulation parameters ranging from isotropic turbulence to a comparatively intensive stratified turbulence. With decreasing Fr, the dissipation

TABLE I. Flow conditions and nondimensional parameters. $\langle u_x \rangle_{xy,\mathrm{rms}}$ is the root-mean-squared (RMS) velocity of the horizontal mean flow. $u_{x,\mathrm{rms}}$ and $u_{z,\mathrm{rms}}$ are RMS velocity fluctuations in the horizontal and vertical directions, respectively. $\omega_{x,\mathrm{rms}}$ and $\omega_{z,\mathrm{rms}}$ are RMS vorticity fluctuations in the horizontal and vertical directions, respectively. T'_{rms} is the RMS temperature fluctuation. ϵ, η, τ_η, $v_\eta (= \eta/\tau_\eta)$, and Re_λ are the dissipation rate, Kolmogorov length scale, Kolmogorov time scale, Kolmogorov velocity scale, and Taylor-scale Reynolds number, respectively. L is the domain length, and κ_m is the maximum wave number. Note that the dissipation rate ϵ is calculated using fluctuation components only. The Prandtl number is set to 7 for all cases considered in this study. Most statistics were obtained from the average over $15,000\tau_\eta$.

Case	$\langle u_x \rangle_{xy,\mathrm{rms}}/v_\eta$	$u_{x,\mathrm{rms}}/v_\eta$	$u_{z,\mathrm{rms}}/v_\eta$	$u_{z,\mathrm{rms}}/u_{x,\mathrm{rms}}$	$\omega_{x,\mathrm{rms}}\tau_\eta$	$\omega_{z,\mathrm{rms}}\tau_\eta$	$T'_{\mathrm{rms}}/\gamma L$	$\epsilon L/v_\eta^3$	$\kappa_m\eta$	$N\tau_\eta$	Re_λ
$\mathrm{Fr} = \infty$	1.069	3.994	3.994	1.00	0.590	0.590	0.310	203.2	1.79	0	60
$\mathrm{Fr} = 1.06$	1.926	3.958	3.047	0.77	0.644	0.526	0.088	194.1	2.05	0.250	52
$\mathrm{Fr} = 0.67$	3.316	3.957	3.816	0.71	0.656	0.479	0.060	195.7	2.05	0.360	54
$\mathrm{Fr} = 0.49$	5.456	3.828	2.504	0.65	0.679	0.448	0.044	186.0	2.11	0.457	54

rate of turbulent kinetic energy is suppressed; thus, the Kolmogorov length and time scales increase slightly. All simulations in Table I were carried out in a periodic cube domain with $L = 2\pi$ and 128 grid points in each direction. The range of Fr is maintained between 0.49 and 1.06 and the Taylor-scale Reynolds number is approximately estimated to be 50 in cases of stratified turbulence. In fact, Yamazaki *et al.* [3] provided turbulent data in ocean thermoclines based on real-site measurement [45], and they used $\mathrm{Re}_\lambda = 38$ targeting the real circumstances of ocean thermoclines in their numerical simulations. Similarly, Wang and Ardekani [6] utilized $\mathrm{Re}_\lambda = 49$ to describe the real stratified ocean. Therefore, the strength of turbulence and stratification in our simulation is in a range comparable with that of the ocean environment. The parameter range of the stratified cases in Table I corresponds to $\epsilon = 10\,\mathrm{cm}^2/s^3$, $v = 0.01\,\mathrm{cm}^2/s$, $\eta = 178\,\mu m$, $\tau_\eta = 31.6\,\mathrm{ms}$ in real units.

In this section, we provide a concise description of stratified turbulence, the statistics of which are summarized in Table I. First, we introduce the "quasi" mean horizontal motion of fluids as defined by an instantaneous large-scale horizontal flow, as follows:

$$\langle u_x \rangle_{xy}(z, t) = \frac{1}{L^2} \int_0^L \int_0^L u_x(\mathbf{x}, t)\, dx\, dy, \quad \langle u_y \rangle_{xy}(z, t) = \frac{1}{L^2} \int_0^L \int_0^L u_y(\mathbf{x}, t)\, dx\, dy, \quad (5)$$

where $\langle \cdot \rangle_{xy}$ denotes the average in the horizontal space. In Fig. 1, example plots of the instantaneous quasi-mean horizontal velocity vector distribution along the vertical direction for the neutral and three different stratified cases at two different instances, normalized by the corresponding lateral RMS velocities, are shown. An observation of this motion yields the result that these horizontal vectors change their directions and local magnitudes randomly in time, while maintaining the same
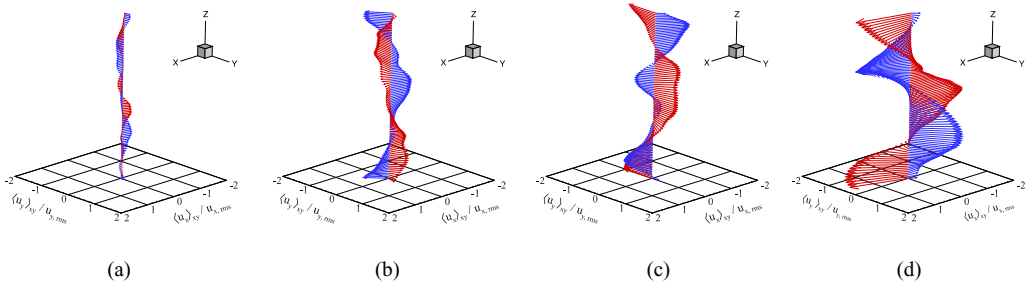

FIG. 1. Instantaneous snapshots of the mean horizontal motion, which are values of horizontal mean velocities normalized by corresponding RMS velocities, are illustrated along the vertical z axis at two representative instances, which are separated from each other by more than $40\tau_\eta$ (red and blue). (a) $\mathrm{Fr} = \infty$, (b) $\mathrm{Fr} = 1.06$, (c) $\mathrm{Fr} = 0.67$, (d) $\mathrm{Fr} = 0.49$.
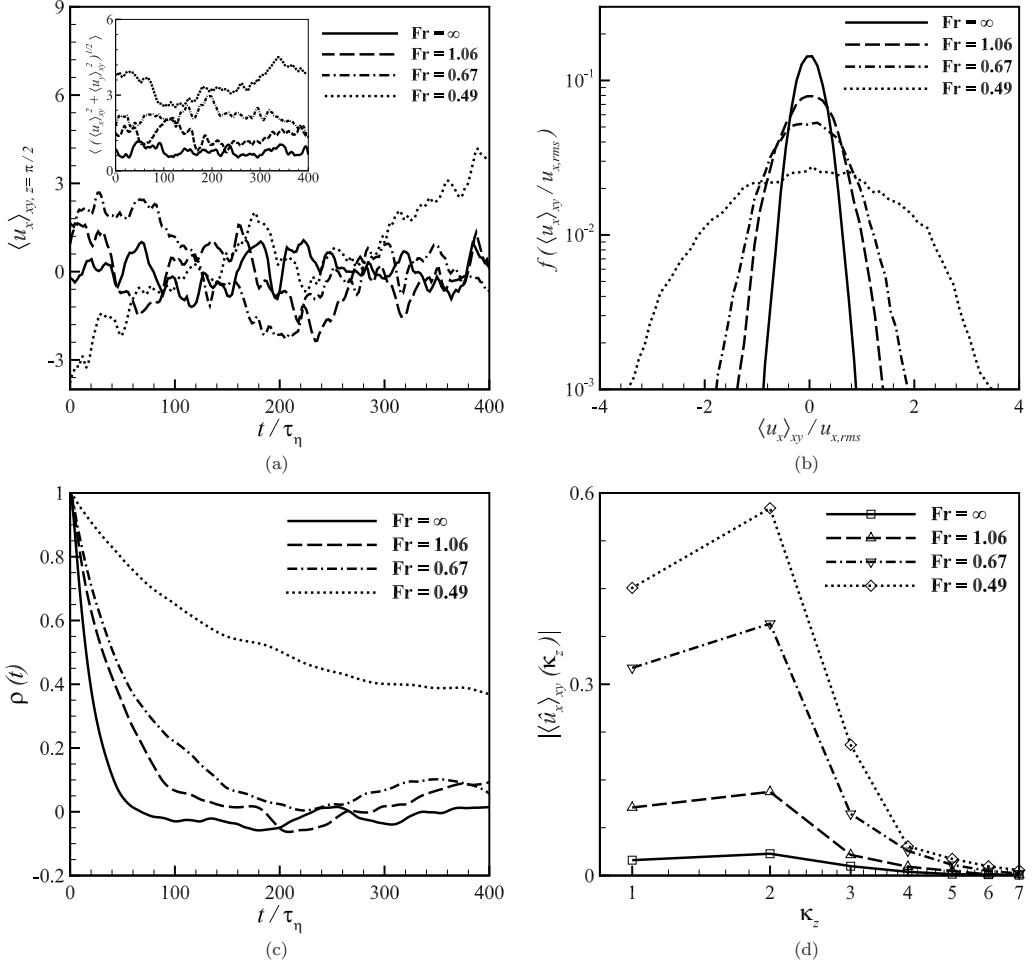
FIG. 2. Statistics of the mean horizontal flow for different stratification strengths, Fr in terms of (a) mean velocity at a specific horizontal plane ($z = \pi/2$) with the magnitude of the mean flow in the inset, (b) probability density function of the mean horizontal flow, $\langle u_x \rangle_{xy}/u_{x,\mathrm{rms}}$, (c) horizontal velocity autocorrelation $\rho(t)$, and (d) the magnitude of the Fourier component of the vertical wave number of the mean horizontal flow.

overall magnitude, as shown in Fig. 2(a). This clearly demonstrates that as the stratification strength increases, the fluctuation range of the mean horizontal flow increases, and the mean horizontal flow persists longer. As the inset shows, the average of the vertical magnitude of this horizontal mean velocity clearly confirms this. Table I also lists the time and vertically averaged magnitude of the horizontal mean velocity. The probability density function distribution of the horizontal mean velocity is shown in Fig. 2(b) and it illustrates that as the stratification becomes stronger, a wider distribution is observed. For the neutral case, with Fr $= \infty$, the PDF exhibits a small but finite width, which is due to the finite size of the simulation domain. For the stratified cases, however, the finite width of PDF is physical. This can be confirmed with the temporal autocorrelation of the mean horizontal velocity, which is clearly shown in Fig. 2(c). Here, the correlation function is defined as follows:

$$\rho(t) = \frac{\langle \langle u_x \rangle_{xy}(t_0, z) \langle u_x \rangle_{xy}(t_0 + t, z) \rangle}{\langle \langle u_x \rangle_{xy}^2 \rangle}, \tag{6}$$
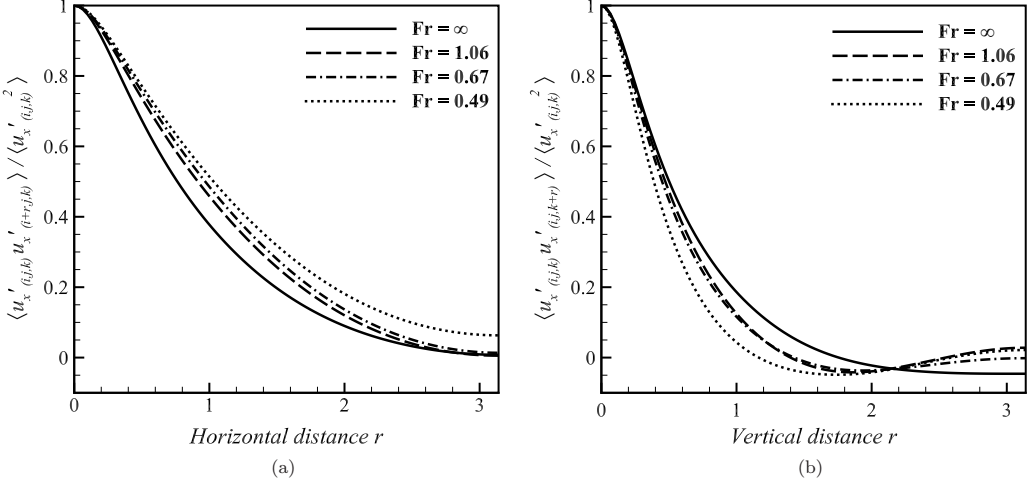
FIG. 3. Spatial correlations of the horizontal fluctuation u_x' along (a) the horizontal direction, and (b) the vertical direction.

where $\langle \cdot \rangle$ denotes the average over time and space (z direction here). To identify the vertical distribution of the mean horizontal motion, the Fourier component of the vertical wave number is investigated in Fig. 2(d). The Fourier component shows a peak value at $\kappa_z = 2$, thereby indicating that on an average, two waves are observed in the vertical domain for the stratified cases. We also tested larger computation domains either horizontally (4π, 4π, 2π) or vertically (2π, 2π, 4π) with the same resolution; however, the overall trend of fluid statistics in Table I is insensitive to the domain size. Although a similar type of layered structure was observed in previous studies [23,25], our analysis clearly indicates that the mean horizontal flow is not steady, however, it persists longer with increasing stratification strength.

With the mean horizontal motion, which has been defined above, varying very slowly in time, we define the horizontal turbulence fluctuations as follows:

$$u_x'(\mathbf{x}, t) = u_x(\mathbf{x}, t) - \langle u_x \rangle_{xy}(z, t), \quad u_y'(\mathbf{x}, t) = u_y(\mathbf{x}, t) - \langle u_y \rangle_{xy}(z, t), \tag{7}$$

with

$$u_{x,\mathrm{rms}} = \sqrt{\langle (u_x')^2 \rangle}, \quad u_{y,\mathrm{rms}} = \sqrt{\langle (u_y')^2 \rangle}, \tag{8}$$

where $\langle \cdot \rangle$ denotes the average over time and space in three dimensions. In Table I, $u_{x,\mathrm{rms}}$, $u_{y,\mathrm{rms}}$ and their ratios are listed. As the stratification increases, both the quantities decrease owing to the emergence of the mean horizontal motion and the horizontal fluctuation becomes dominant over the vertical fluctuation. The horizontal and vertical correlations of the horizontal fluctuations shown in Fig. 3 indicate that as stratification intensifies, the horizontal correlation increases while the vertical correlation decreases, thereby implying that the scales of eddy motion become anisotropic. The aforementioned trend can be observed in Fig. 4, which depicts that the instantaneous vorticity contours of ω_y in the x-z plane for different stratification strengths. As the stratification intensifies, the vortical structures become more stretched in the horizontal direction. The RMS vorticity in the horizontal and vertical directions listed in Table I clearly confirms that this anisotropic nature of vorticity is intensified with a decrease in Froude number.
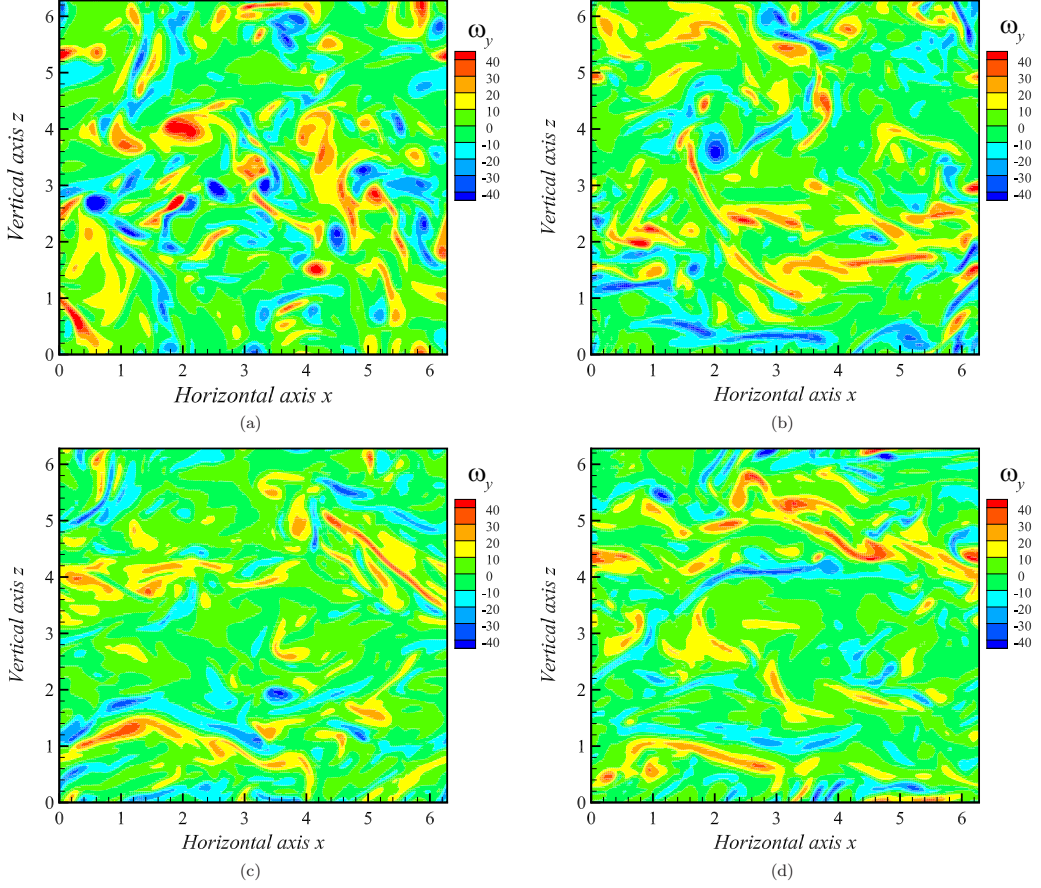
FIG. 4. Instantaneous vorticity contours (ω_y) of the fluctuation field in the x-z plane ($y = \pi/2$). (a) Fr $= \infty$, (b) Fr $= 1.06$, (c) Fr $= 0.67$, (d) Fr $= 0.49$.

For the investigation of scale modification by stratification, the one-dimensional spectra in the horizontal and vertical directions are illustrated in Fig. 5, where the spectra are defined by

$$E_x(\kappa_h) = \sum_{\kappa_x} \frac{1}{2}(|\hat{u}'_x(\kappa_x)|^2 + |\hat{u}'_y(\kappa_x)|^2), \quad E_x(\kappa_v) = \sum_{\kappa_z} \frac{1}{2}(|\hat{u}'_x(\kappa_z)|^2 + |\hat{u}'_y(\kappa_z)|^2), \qquad (9)$$

where E_x is the one-dimensional energy spectrum of the horizontal velocities, and κ_x and κ_z are the horizontal and vertical wave numbers, respectively. As the stratification intensifies, a steeper horizontal spectrum is observed, thereby implying that small-scale motions are suppressed to a greater degree as compared to the large-scale motions, as shown in Fig. 5(a). This attenuation of small-scale motions leads to a break into a higher slope. This is obviously caused by the enhanced elongation of structures in the horizontal direction by stratification shown in Fig. 5. In contrast, an observation of the vertical spectrum shown in Fig. 5(b), yields the result that large-scale motion is slightly suppressed by stratification when small-scale motions are enhanced, as shown in the inset.

For the completeness of statistical investigation, the statistics of temperature fluctuation $T'(x, y, z, t)$ were obtained. The horizontally averaged temperature fluctuation, $\langle T'\rangle_{xy}(z, t) \sim 0$ everywhere, indicating that the horizontally dominant motion of fluid does not cause any kind of layered temperature structure. The RMS of temperature fluctuation, $T'_{\rm rms}$, is listed in Table I for all cases, suggesting that the RMS fluctuation of temperature is suppressed by stratification.
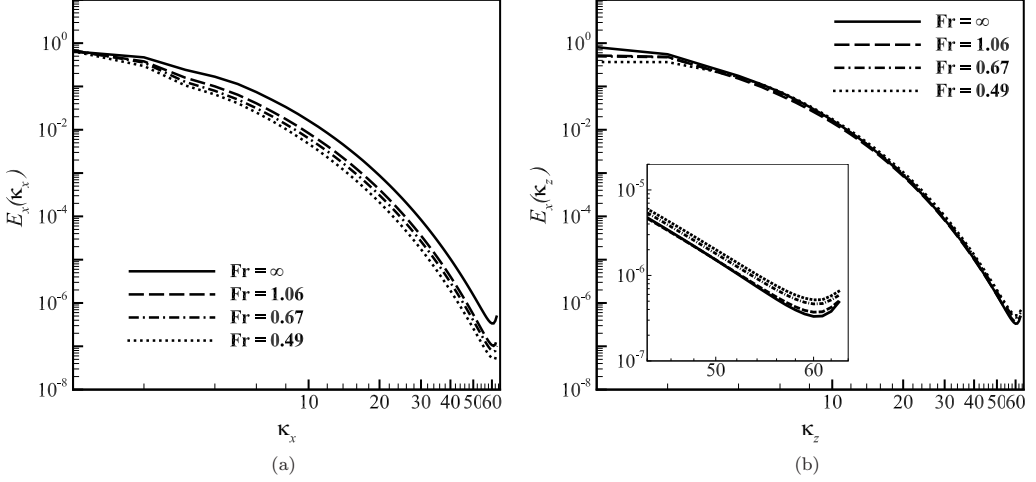
FIG. 5. One-dimensional horizontal kinetic energy spectra E_x depending on (a) a horizontal wave number κ_x, (b) a vertical wave number κ_z with the inset of a maximum wave number regime. By descending Fr, E_x is lowered considerably on the horizontal wave number κ_x. On the vertical wave number κ_z, the gap between E_x can hardly be seen, except for in the inset, where the small-scale energy drops with attenuating stratification.

III. BEHAVIOR OF MICROBUBBLES IN STRATIFIED TURBULENCE

The motion of small spherical bubbles in isotropic turbulence has been studied over a long period. Especially, the effect of lift forces on spherical bubbles was described in Refs. [46,47]. Here, we investigate the behavior of microbubbles in stratified turbulence. The equation of motion, including the lift forces, was proposed by Refs. [27–29],

$$\frac{d\boldsymbol{v}}{dt} = 3\frac{D\boldsymbol{u}}{Dt} - \frac{1}{\tau_b}(\boldsymbol{v} - \boldsymbol{u}) - 2\boldsymbol{g} - (\boldsymbol{v} - \boldsymbol{u}) \times \boldsymbol{\omega}, \qquad (10)$$

where $\boldsymbol{v}$, $\boldsymbol{u}$, $D\boldsymbol{u}/Dt$, τ_b, $\boldsymbol{\omega}$ represent the bubble velocity, fluid velocity at the bubble's position, fluid acceleration at the bubble's position, the bubble response time, vorticity of the fluid at the bubble's position, respectively. The response time of a bubble in terms of its bubble radius a, fluid viscosity, and the bubble Reynolds number Re_b is given by $\tau_b = a^2/6\nu r$, with $r = 1 + 0.16\mathrm{Re}_b^{0.5}$ [28], where $\mathrm{Re}_b = 2|\boldsymbol{v} - \boldsymbol{u}|a/\nu$ is the bubble Reynolds number. In Eq. (10), the forces acting on the bubbles are the fluid acceleration due to the added mass effect, the drag force, buoyancy, and the lift force, respectively. A lift force coefficient of 0.5 is adopted, which is valid in the range of $1 \sim \mathrm{Re}_b \leqq 100$ [27,28,46–48]. The valid range of Re_b for the drag force is $\mathrm{Re}_b \leqq 100$ [27,28,48]. The Stokes number is defined by $\mathrm{St} = \tau_b/\tau_\eta = (a/\eta)^2/6r$, suggesting that the point-bubble approximation $(a/\eta < 1)$ indeed restricts the Stokes number, $\mathrm{St} \ll 1$. Table II lists the bubble parameters for the two different sizes of bubbles considered in our simulation; $a/\eta = 0.55$ and 0.78, which corresponds to $a = 98\,\mu m$ and $a = 138\,\mu m$ in real units, respectively. The buoyancy number W is defined by $W = V_T/v_\eta$, where $V_T(= 2\tau_b g)$ denotes the bubble rise velocity in still fluid. The bubble Reynolds number Re_b is estimated based on V_T and falls within the valid range of $1 \sim \mathrm{Re}_b \leqq 100$ as shown in Table II. The number of bubbles N_b is 100,000, which is sufficient for analyzing the behavior of bubbles. As Eq. (10) targets free-surfactant spherical bubbles in the derivation of the drag force [27,28], we assume that no impurities exist on the bubble's surface and in the fluids, so that the fluid can slip on the bubble's surface. Note that the equation of motion for bubbles is valid for $2a = 120 \sim 250\,\mu m$ [27,29], and thus the range of St for microbubbles is usually estimated to be below 0.1 in most circumstances. To obtain fully developed bubble statistics, we initially released bubbles uniformly in the periodic domain. After developing fluid and bubbles for $100\tau_\eta$, which is a

TABLE II. Parameters of bubbles and some statistics of bubbles for four different strengths of stratification. $\mathrm{St}(= \tau_b/\tau_\eta = (a/\eta)^2/6r)$ and $W(= V_T/v_\eta)$ represent the Stokes number and buoyancy number, respectively. Note that $V_T(= 2\tau_b g)$ denotes the rise velocity of bubbles in still fluid, v_η is the Kolmogorov velocity scale. T_L^x means the Lagrangian integral timescale in the horizontal direction. $\langle v_x \rangle_{\mathrm{rms}}$, $\langle v_z \rangle$ denote the averaged horizontal r.m.s. velocity of the bubbles, and the averaged rise velocities of the bubbles in turbulence, respectively. $\langle \Omega \rangle_b$ and $\langle \Omega \rangle$ are averaged values of the fluid enstrophy at the bubble's positions and the Eulerian average enstrophy, respectively.

a	St	W	Re_b	Fr	T_L^x/τ_b	$\langle v_x \rangle_{\mathrm{rms}}/V_T$	$\langle \Omega \rangle_b/\langle \Omega \rangle$	$(\langle v_z \rangle - V_T)/V_T$
0.55η	0.05	5.5	$5.9 \sim 6.0$	∞	63.6	0.74	1.19	-0.071
				1.06	46.4	0.83	1.09	-0.054
				0.67	28.0	0.87	1.06	-0.035
				0.49	20.4	1.06	1.04	-0.022
0.78η	0.1	11.0	$16.7 \sim 17.4$	∞	22.7	0.37	1.19	-0.070
				1.06	16.1	0.41	1.06	-0.046
				0.67	8.8	0.44	1.05	-0.032
				0.49	6.8	0.53	1.03	-0.021

sufficient amount of time, various statistics of the bubbles were calculated. For the parameter range of the current study, the height of the domain is sufficient to ensure that rising bubbles encounter decorrelated fluid information.

It is well known that bubbles are trapped in high vorticity regions and preferably collected at the downwelling side [28]. Convoluted motions of bubbles due to a combination of added mass effects, drag, buoyancy, and lift have been analyzed in isotropic turbulence through experiments and numerical simulations [27–29,33]. The behavior of bubbles in stratified turbulence, however, has rarely been studied in contrast to heavy particles, whose behavior in stratified turbulence has been well investigated [21,23,24]. Although the dynamic characteristics of heavy particles and bubbles are different in principle, whether heavy particles or bubbles cluster in preferential regions forms an important research question. Table II provides some statistics related to bubble behavior in stratified turbulence such as the enstrophy ratio and a modification in the rise velocities for bubbles of two different sizes with four different stratification strengths, including a neutral one. The enstrophy ratio $\langle \Omega \rangle_b/\langle \Omega \rangle$ indicates the ratio of the averaged enstrophy of the fluid at the bubbles' positions $\langle \Omega \rangle_b (= \langle \omega_b^2 \rangle/2)$ and the Eulerian average enstrophy of the fluid $\langle \Omega \rangle (= \langle \omega_E^2 \rangle/2)$. ω_b and ω_E denote the RMS fluid vorticity at the bubble's position and at the Eulerian grids, respectively. If this ratio is greater than 1, then the bubbles are more likely to be located in high vorticity regimes [27–29]. Although the clustering of bubbles is weak, because the enstrophy ratios shown in Table II are not far from 1, we observe a slight attenuation of clustering as the stratification becomes stronger. The reduction rate $(\langle v_z \rangle - V_T)/V_T$ which is the ratio of the rise velocity of the bubbles in turbulence $\langle v_z \rangle$ relative to that in a quiescent fluid V_T also yields the same conclusion. As Fr decreases, the rise velocity of the bubbles tends to recover that in still fluid as shown in Table II. Combining alterations of the enstrophy ratio and the rise velocity confirms that bubbles cannot be effectively trapped when the stratification is strong, owing to the anisotropic structures of the fluid. Fig. 6 indeed indicates that whether stratified or not, a clustering of bubbles can hardly be noticed for the range of Re_b. It can be conjectured that the mean oscillatory horizontal flow of fluids accompanied by vortical structures shown in Fig. 6 might deprive bubbles of a chance to interact with vortical structures.

To understand the behavior of bubbles in stratified turbulence in detail, we investigate the modification in the bubble's trajectories. Figure 7 illustrates the trajectories of three bubbles in isotropic turbulence (Fr $= \infty$) and the most stratified turbulence (Fr $= 0.49$). Compared with the natural meandering motions of rising bubbles due to turbulence shown in Fig. 7(a), the bubbles in
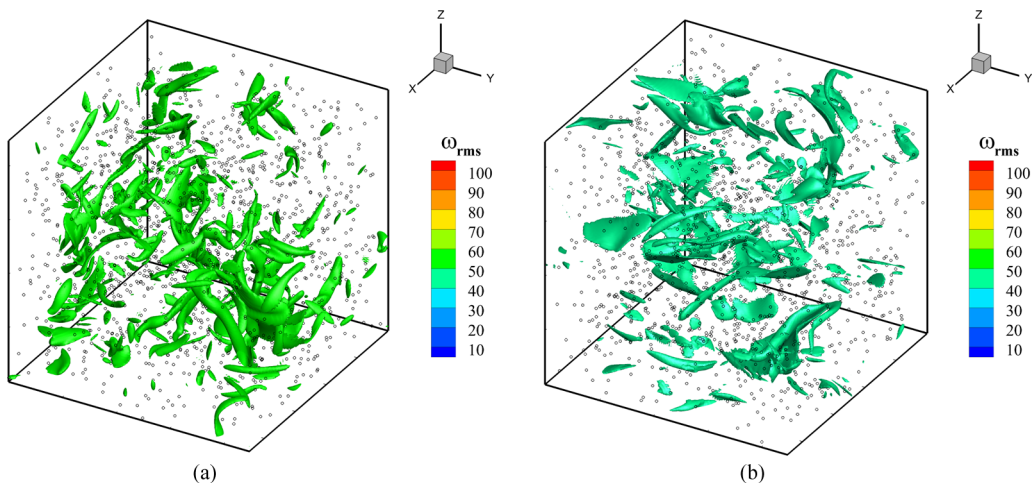
FIG. 6. Vorticity isosurface with a sample of 2000 bubbles with $a = 0.78\eta$. (a) Fr $= \infty$, (b) Fr $= 0.49$. Clustering of bubbles in preferential regions is barely observed for Re$_\lambda \sim 50$–60.

stratified turbulence exhibit a strongly sinuous motion, as shown in Fig. 7(c). The two-dimensional projection of those trajectories shown in Figs. 7(b) and 7(d) clearly indicates that all three bubbles in stratified turbulence tend to oscillate from side to side in a synchronized pattern unlike the bubbles in isotropic turbulence, although the bubbles are horizontally separated by more than half of a domain length. This sinuous motion is caused by the layered structure of fluid motion discussed above.

Figure 8 shows temporal autocorrelations of bubbles' horizontal velocity and the corresponding frequency spectra for two sizes of bubbles in four different stratified flows. The autocorrelation functions $\rho_b(t)$ and spectra $\varphi(\omega)$ are defined by

$$\rho_b(t) = \frac{1}{N_p} \sum^{N_p} \frac{1}{2} \left(\frac{\langle v_x(t_0) v_x(t_0 + t) \rangle}{\langle v_x(t_0)^2 \rangle} + \frac{\langle v_y(t_0) v_y(t_0 + t) \rangle}{\langle v_y(t_0)^2 \rangle} \right) \tag{11}$$

$$\varphi(\omega) = \int_0^\infty \rho_b(t) \cos(\omega t) dt \tag{12}$$

where the average was over 100 000 bubbles. As shown in Figs. 8(a) and 8(c), the autocorrelation shows oscillatory behavior for all stratified cases considered and the amplitude decays in time more slowly with increasing stratification strength. The corresponding spectrum shown in Figs. 8(b) and 8(d) clearly indicate a strong peak at $\omega\tau_\eta = 0.18$ and $\omega\tau_\eta = 0.35$, respectively for two different sizes of bubbles. Because the rise velocity of the larger bubbles ($a = 0.78\eta$) is roughly twice of that of the smaller bubbles ($a = 0.55\eta$), the dominant frequency of the larger bubbles is found to be roughly twice the value of the smaller ones. It can also be observed that the dominant peak shifts toward a slightly higher frequency with decreasing Fr because the bubble rise velocity is more likely to be restored toward the rise velocity in still fluid by the oscillatory mean flows, as listed in Table II. It should be noted that these zigzag patterns are not caused by the wake instability discussed in Ref. [36].

Single-bubble dispersion aids in the understanding of diffusion over time in bubble-laden turbulence. Single-particle dispersion of heavy particles in stratified turbulence was fully investigated in a series of studies [21–23,25]. They reported the effects of St on the horizontal and vertical dispersion for different stratification strengths. When gravity was not considered in the motion of particles, their horizontal dispersion in stratified turbulence generally maintained a t^2 slope at all times, whereas their vertical one started with t^2 and eventually changed to a t^1 slope as time progressed. If the particles are affected by gravity [22], then the horizontal dispersion of heavy particles gradually
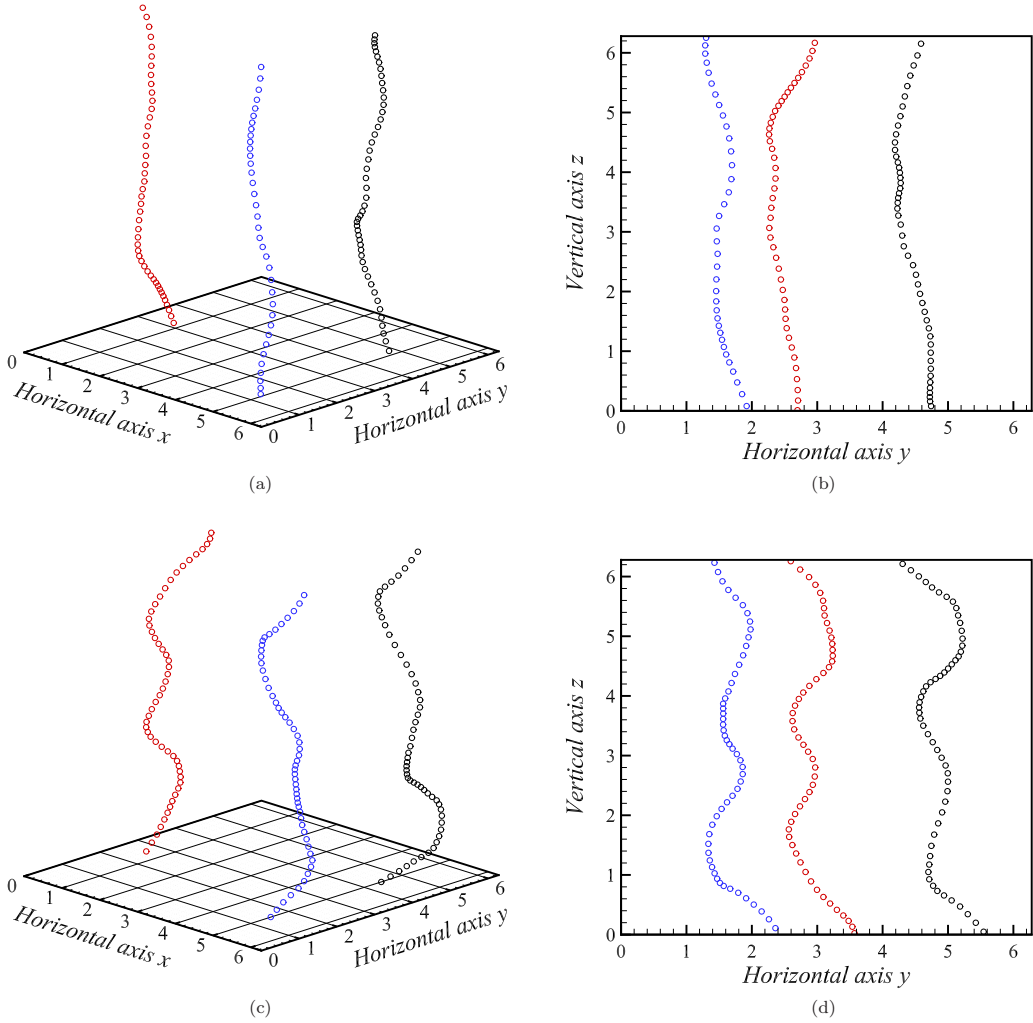
FIG. 7. Trajectory of certain bubbles($a = 0.78\eta$) in turbulence when (a) Fr $= \infty$ (three-dimension), (b) Fr $= \infty$ (two-dimension), (c) Fr $= 0.49$ (three-dimension), (d) Fr $= 0.49$ (two-dimension). The bubbles are more likely to rise up undulated at strong stratification.

declines to a slope of t^1 as the gravitational force increases. In our case, Fig. 9 depicts the horizontal mean-square displacement of the bubbles $\langle [x(t) - x(0)]^2 \rangle / \eta^2$ for both sizes of bubbles, where $x(t)$ and $x(0)$ are the bubble's horizontal positions at time t and their initial positions, respectively. In isotropic turbulence, rising bubbles of both sizes show a horizontal dispersion proportional to t^2 in the initial stage and then t^1 at a later point in time. In stratified turbulence, however, the horizontal dispersion of rising bubbles at the later stage is suppressed, and the slope reduces to 5/7 at Fr $= 0.49$. Note that the slope 5/7 is an observed value, indicating that this late-stage diffusion is sub-diffusion. The behavior is clearly demonstrated by the inset in a linear scale. Owing to the oscillatory motion of the background stratified fluid, the oscillations were observed in the dispersion for both sizes of the bubbles. This suppression of horizontal dispersion by stratification does not follow intuitively, given that stratification induces the quasi-mean horizontal motion, as discussed in the previous section. It can be conjectured that although the mean horizontal motion is caused by stratification, the dispersion due to this mean motion is quite limited because it is periodic, not
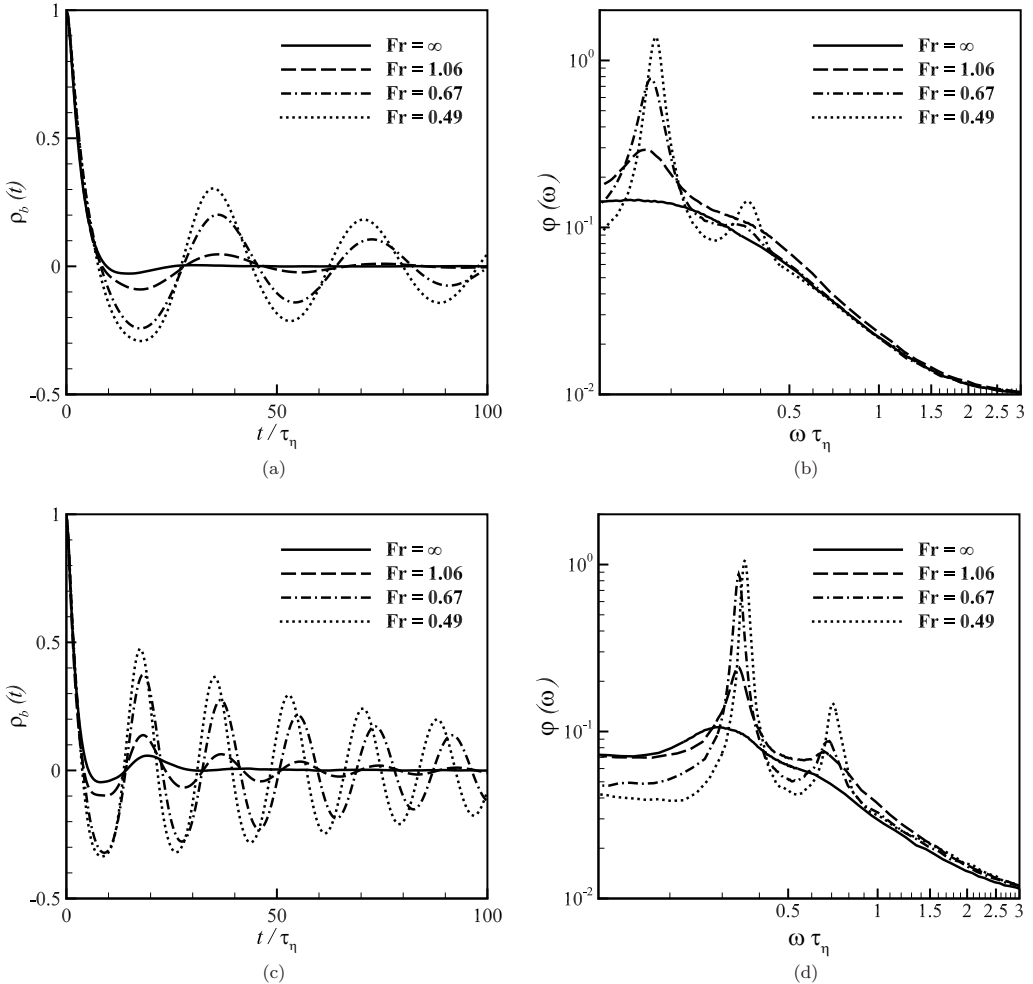
FIG. 8. Horizontal velocity autocorrelations of each bubble ($N_b = 100\,000$) and conversions into the frequency domain. $a = 0.55\eta$ in the (a) time domain, (b) frequency domain, and $a = 0.78\eta$ in the (c) time domain, (d) frequency domain. When Fr becomes smaller, a growth in correlation with $\varphi(\omega)$ is observed around the dominant frequency regimes. As the bubble becomes larger, the dominant frequencies are ousted to higher ones.

random. It is also noted that larger bubbles disperse more slowly than small bubbles owing to faster rising motion and this trend is more pronounced in stratified turbulence.

Finally, we investigate the relative dispersion of a pair of bubbles, which is one of key factors in identifying the characteristics of spreading particles in fluids. Several studies have been conducted with the aim of recognizing a relationship between turbulence and particles by tracking coupled particles. Ni and Xia [49] performed an experiment in turbulent thermal convection by differentiating the initial distances between fluid particles. They reported power-law growth regimes of paired particles, which is termed the Batchelor regime ($\sim t^2$) and the Richardson regime ($\sim t^3$). They also discovered that the separation of the fluid particles augments as the initial distance increases. Mazzitelli and Lohse [29] investigated the separation characteristics of paired bubbles in isotropic turbulence by direct numerical simulations and claimed that there are three regimes of power-law growth (sequentially, the Batchelor, Richardson, and t^1) of the bubbles' separation as
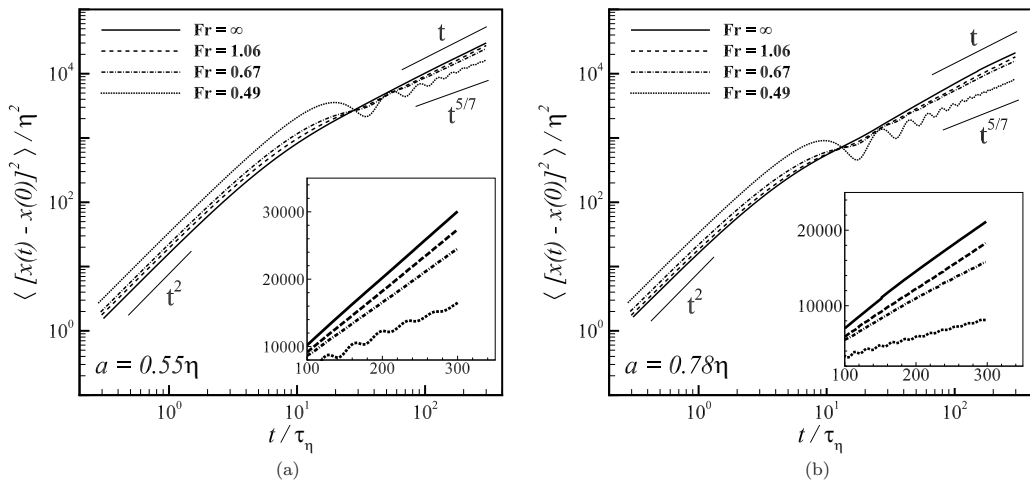
FIG. 9. The horizontal mean-square displacement $\langle [x(t) - x_0]^2 \rangle / \eta^2$ of bubbles as a function of time is computed for (a) $a = 0.55\eta$, (b) $a = 0.78\eta$. 100 000 bubbles are tracked individually from their initial positions onward. During the early stage, the displacement increases with t^2 in all cases. After t increases to more than $20\tau_\eta$, the slope changes to approximately t^1, and shows a smaller displacement at a lower Fr.

time passes. Here, we identify the separation of bubbles for different strengths of stratification by varying the initial horizontal distance between paired bubbles. Figure 10 describes the temporal separation $\langle [r_x(t) - r_x(0)]^2 \rangle / \eta^2$ between paired bubbles, where $r_x(t)$ is the horizontal distance between paired bubbles at a specific time t with $r_x(0)$ being the initial horizontal distance. We considered two different initial distances, $r_x(0) = 2\eta$ and 20η. Figures 10(a) and 10(b) show $\langle [r_x(t) - r_x(0)]^2 \rangle / \eta^2$ for two initial distances and two sizes of paired bubbles in isotropic turbulence and in the most stratified turbulence, respectively. As discussed in Ref. [29], the overall trends of power-growth are shown in three regimes. At a small separation time with $t < \tau_\eta$, the Batchelor regime (t^2) is observed for all $r_x(0)$. As time progresses, the Richardson regime (t^3) appears in case of $r_x(0) = 2\eta$ at $a = 0.55\eta$ in both isotropic and stratified turbulence (this regime is not seen for $a = 0.78\eta$ owing to a decline in the power-law at high W [29]). At large a separation time $t \approx 100\tau_\eta$, the slope behaves approximately t^1 for both initial distances and for both sizes of bubbles. For a larger initial separation, both sizes of bubbles show typical ballistic-to-diffusive transition. For small initial distances, larger bubbles have a bigger pair separation until $t < \tau_\eta$. However, this trend is overturned as time goes. As time goes over τ_η, larger bubbles diffuse slower than small bubbles due to high rise velocity. The effect of stratification on pair dispersion is also investigated in Figs. 10(c) and 10(d). It is seen that pair separation tends to become weaker as stratification becomes stronger for both initial distances (see insets drawn in a linear scale). Therefore, it can be asserted that the bubbles slowly diffuse as the stratification intensifies, and this tendency does not rely on their initial distances, while maintaining three-regime behavior for a small initial separation and the ballistic-to-diffusive transition for a large initial separation. For a large initial separation, $r_x(0) = 20\eta$, which is in the inertial range, the transition occurs at the Batchelor time scale, $t_0 \{= [r_x^2(0)/\epsilon]^{1/3}\}$ with $t_0/\tau_\eta = 7.3 \sim 7.7$ for all stratified cases, as shown in Fig. 10(d).

IV. CONCLUSION

We investigated the dynamics of microbubbles in stratified turbulence by direct numerical simulation. To identify the dynamic behaviors of bubbles, a detailed analysis of stratified turbulence was performed, and it was compared with the results of isotropic turbulence. To describe stratified turbulence, we introduced horizontally averaged oscillatory mean motions that vary in time but
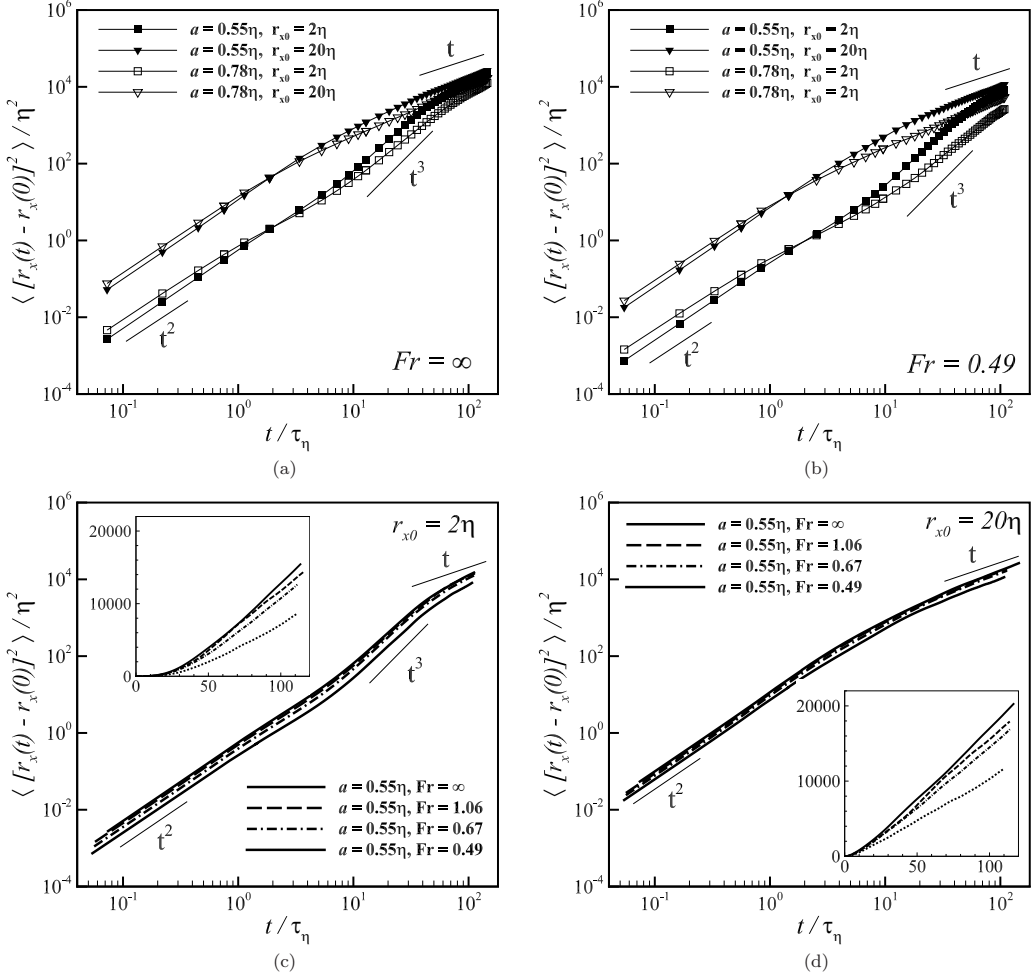
FIG. 10. Horizontal mean-square separation $\langle [r_x(t) - r_x(0)]^2 \rangle / \eta^2$ of paired bubbles as a function of time. Initially, 50 000 pairs of bubbles ($N_b = 100\,000$) are horizontally distributed with two initial distances $r_x(0)$ between any pair of bubbles: 2η (square symbol), 20η (triangle symbol). Pair separations for two sizes of bubbles $a = 0.55\eta$ (solid symbol), $a = 0.78\eta$ (hollow symbol) are presented for (a) Fr $= \infty$, (b) Fr $= 0.49$. As the initial distance $r_x(0)$ grows, the horizontal separation also increases. We also represent the stratification effects for $a = 0.55\eta$ in conditions of (c) $r_x(0) = 2\eta$, (d) $r_x(0) = 20\eta$ in the insets in a linear scale. The separation is suppressed by stratification.

persist longer as the stratification is increased. This layered structure is well-recognized in the distribution of vortical structures. Fluctuations from this mean motion are strongly anisotropic. Spatial correlations of the fluctuations indicate that the horizontal scales become larger as stratification is increased, whereas the vertical scales become smaller.

We observed that a clustering of bubbles is rarely observed at $Re_\lambda = 50$–60 when St is below 0.1. In particular, we discovered that the bubbles are hardly trapped in the high vorticity regions as the stratification is increased. Owing to a suppressed clustering, the rise velocity of bubbles almost recovers to that seen in a quiescent fluid in stratified turbulence. The bubbles tend to rise in a zigzag pattern, not necessarily in the same plane, in stratified turbulence. Temporal correlations of a bubble's horizontal velocity and the corresponding spectrum clearly indicated that there exists

a dominant frequency. This trend is more prominent with stronger stratification and with larger bubbles (with higher St and W).

The diffusion behavior of bubbles in stratified turbulence was also investigated. In the case of single-bubble dispersion, we noticed that the bubbles horizontally disperse with a rate of t^2 during the early stage. Then, this rate is altered to t^1 for isotropic turbulence, and it decreases as stratification increases. More interestingly, the horizontal dispersion is suppressed by stratification, which was caused by the oscillatory mean motion that is not random. In the pair dispersion investigation, we observed that there exists a power-law growth, such as the Batchelor (t^2), Richardson(t^3), and t^1 regimes for a small initial separation [$r_x(0) = 2\eta$], but the regime of Richardson is hardly observed with a large initial separation [$r_x(0) = 20\eta$]. We also noted that as the stratification increases, the separation of pairs is slowly broadened for the same initial distance, indicating that the relative diffusion is suppressed by stratification.

Finally, we mention that unlike heavy inertial particles, the point-bubble approximation is valid only for St $\ll$ 1, which limits the range of parameters. For this reason, the diverse behavior of bubbles is unobservable. Although the point-bubble approximation is an effective tool to describe the motion of microbubbles, there are limitations to describing finite-size bubbles and deformable bubbles, or to account for the effect of volume fraction [27,28]. A proper approach to describe the dynamics of finite-size bubbles would involve the use of an immersed boundary method [50–52]. However, the behavior of rising bubbles in stratified turbulence is clearly different from that of heavy settling particles. The meandering motion of bubbles could influence the background stratified turbulence if the two-way interaction is considered, which could be a good topic for a future study.

---

[1] J. Magnaudet and M. J. Mercier, Particles, drops, and bubbles moving across sharp interfaces and stratified layers, Ann. Rev. Fluid Mech. **52**, 61 (2020).

[2] V. Mathai, D. Lohse, and C. Sun, Bubbly and buoyant particle-laden turbulent flows, Ann. Rev. Condens. Matter Phys. **11**, 529 (2020).

[3] H. Yamazaki, T. R. Osborn, and K. D. Squires, Direct numerical simulation of planktonic contact in turbulent flow, J. Plankton Res. **13**, 629 (1991).

[4] B. J. Rothschild and T. R. Osborn, Small-scale turbulence and plankton contact rates, J. Plankton Res. **10**, 465 (1988).

[5] C. Marrase, J. H. Costello, T. Granata, and J. R. Strickler, Grazing in a turbulent environment: Energy dissipation, encounter rates, and efficacy of feeding currents in *Centropages hamatus*, Proc. Natl. Acad. Sci. USA **87**, 1653 (2006).

[6] S. Wang and A. M. Ardekani, Biogenic mixing induced by intermediate Reynolds number swimming in stratified fluids, Sci. Rep. **5**, 17448 (2015).

[7] G. L. Wagner, W. R. Young, and E. Lauga, Mixing by microorganisms in stratified fluids, J. Mar. Res. **72**, 47 (2014).

[8] T. Gerz and H. Yamazaki, Direct numerical simulation of buoyancy-driven turbulence in stably stratified fluid, J. Fluid Mech. **249**, 415 (1993).

[9] Y. Kimura and J. R. Herring, Diffusion in stably stratified turbulence, J. Fluid Mech. **328**, 253 (1996).

[10] H. J. Kaltenbach, T. Gerz, and U. Schumann, Large-eddy simulation of homogeneous turbulence and diffusion in stably stratified shear flow, J. Fluid Mech. **280**, 1 (1994).

[11] W. R. Peltier and C. P. Caulfield, Mixing efficiency in stratified shear flows, Annu. Rev. Fluid Mech. **35**, 135 (2003).

[12] E. D. Gonzalez-Juez, A. R. Kerstein, and L. H. Shih, Vertical mixing in homogeneous sheared stratified turbulence: A one-dimensional-turbulence study, Phys. Fluids **23**, 055106 (2011).

[13] Y. G. Park, J. A. Whitehead, and A. Gnanadeskian, Turbulent mixing in stratified fluids: Layer formation and energetics, J. Fluid Mech. **279**, 279 (1994).

[14] S. E. Holt and J. H. Ferziger, A numerical study of the evolution and structure of homogeneous stably stratified sheared turbulence, J. Fluid Mech. **237**, 499 (1992).

[15] P. Piccirillo and C. W. Van Atta, The evolution of a uniformly sheared thermally stratified turbulent flow, J. Fluid Mech. **334**, 61 (1997).

[16] M. L. Waite, Stratified turbulence at the buoyancy scale, Phys. Fluids **23**, 066602 (2011).

[17] G. Brethouwer, P. Billant, E. Lindborg, and J. M. Chomaz, Scaling analysis and simulation of strongly stratified turbulent flows, J. Fluid Mech. **585**, 343 (2007).

[18] L. H. Shih, J. R. Koseff, J. H. Ferziger, and C. R. Rehmann, Scaling and parametrization of stratified homogeneous turbulent shear flow, J. Fluid Mech. **412**, 1 (2000).

[19] D. Chung and G. Matheou, Direct numerical simulation of stationary homogeneous stratified sheared turbulence, J. Fluid Mech. **696**, 434 (2012).

[20] A. Pumir, Turbulence in homogeneous shear flows, Phys. Fluids **8**, 3112 (1996).

[21] M. van Aartrijk and H. J. Clercx, Vertical dispersion of light inertial particles in stably stratified turbulence: The influence of the Basset force, Phys. Fluids **22**, 013301 (2010).

[22] M. van Aartrijk and H. J. Clercx, Dispersion of heavy particles in stably stratified turbulence, Phys. Fluids **21**, 033304 (2009).

[23] M. van Aartrijk and H. J. Clercx, The dynamics of small inertial particles in weakly stratified turbulence, J. Hydro-Environment Res. **4**, 103 (2010).

[24] M. Van Aartrijk and H. J. Clercx, Preferential Concentration of Heavy Particles in Stably Stratified Turbulence, Phys. Rev. Lett. **100**, 254501 (2008).

[25] M. van Aartrijk, H. J. Clercx, and K. B. Winters, Single-particle, particle-pair, and multiparticle dispersion of fluid particles in forced stably stratified turbulence, Phys. Fluids **20**, 025104 (2008).

[26] A. Eidelman, T. Elperin, N. Kleeorin, B. Melnik, and I. Rogachevskii, Tangling clustering of inertial particles in stably stratified turbulence, Phys. Rev. E **81**, 056313 (2010).

[27] I. M. Mazzitelli, D. Lohse, and F. Toschi, The effect of microbubbles on developed turbulence, Phys. Fluids **15**, L5 (2003).

[28] I. M. Mazzitelli, D. Lohse, and F. Toschi, On the relevance of the lift force in bubbly turbulence, J. Fluid Mech. **488**, 283 (2003).

[29] I. M. Mazzitelli and D. Lohse, Lagrangian statistics for fluid particles and bubbles in turbulence, New J. Phys. **6**, 203 (2004).

[30] L. P. Wang and M. R. Maxey, The motion of microbubbles in a forced isotropic and homogeneous turbulence, Appl. Sci. Res. **51**, 291 (1993).

[31] M. R. Maxey, E. J. Chang, and L. P. Wang, Simulation of interactions between microbubbles and turbulent flows, Appl. Mech. Rev. **47**, S70 (1994).

[32] E. Calzavarini, M. Kerscher, D. Lohse, and F. Toschi, Dimensionality and morphology of particle and bubble clusters in turbulent flow, J. Fluid Mech. **607**, 13 (2008).

[33] A. Aliseda and J. C. Lasheras, Preferential concentration and rise velocity reduction of bubbles immersed in a homogeneous and isotropic turbulent flow, Phys. Fluids **23**, 093301 (2011).

[34] J. M. Mercado, V. N. Prakash, Y. Tagawa, C. Sun, and D. Lohse, Lagrangian statistics of light particles in turbulence, Phys. Fluids **24**, 055106 (2012).

[35] V. Mathai, E. Calzavarini, J. Brons, C. Sun, and D. Lohse, Microbubbles and Microparticles are Not Faithful Tracers of Turbulent Acceleration, Phys. Rev. Lett. **117**, 024501 (2016).

[36] E. Alméras, V. Mathai, D. Lohse, and C. Sun, Experimental investigation of the turbulence induced by a bubble swarm rising within incident turbulence, J. Fluid Mech. **825**, 1091 (2017).

[37] M. Bourgoin, N. T. Ouellette, H. Xu, J. Berg, and E. Bodenschatz, The role of pair dispersion in turbulent flow, Science **311**, 835 (2006).

[38] M. Bourgoin, Turbulent pair dispersion as a ballistic cascade phenomenology, J. Fluid Mech. **772**, 678 (2015).

[39] V. Mathai, S. G. Huisman, C. Sun, D. Lohse, and M. Bourgoin, Dispersion of Air Bubbles in Isotropic Turbulence, Phys. Rev. Lett. **121**, 054501 (2018).

[40] J. T. Kim, J. Nam, S. Shen, C. Lee, and L. P. Chamorro, On the dynamics of air bubbles in Rayleigh-Bénard convection, J. Fluid Mech. **891**, A7 (2020).

[41] P. R. Thompson, C. G. Piecuch, M. A. Merrifield, J. P. McCreary, and E. Firing, Forcing of recent decadal variability in the Equatorial and North Indian Ocean, J. Geophys. Res.: Oceans **121**, 6762 (2016).

[42] J. H. Liang, C. Deutsch, J. C. McWilliams, B. Baschek, P. P. Sullivan, and D. Chiba, Parameterizing bubble-mediated air-sea gas exchange and its effect on ocean ventilation, Global Biogeochem. Cycles **27**, 894 (2013).

[43] T. Ito and C. Deutsch, Understanding the saturation state of argon in the thermocline: The role of air-sea gas exchange and diapycnal mixing, Global Biogeochemical Cycles **20**, 1 (2006).

[44] C. C. Henning, D. Archer, and I. Fung, Argon as a tracer of cross-isopycnal mixing in the thermocline, J. Phys. Oceanogr. **36**, 2090 (2006).

[45] L. R. Haury, H. Yamazaki, and E. C. Itsweire, Effects of turbulent shear flow on zooplankton distribution, Deep-Sea Res. Part A: Oceanogr. Res. Papers **37**, 447 (1990).

[46] D. Legendre and J. Magnaudet, The lift force on a spherical bubble in a viscous linear shear flow, J. Fluid Mech. **368**, 81 (1998).

[47] R. T. Auton, The lift force on a spherical body in a rotational flow, J. Fluid Mech. **183**, 199 (1987).

[48] I. Fouxon, G. Shim, S. Lee, and C. Lee, Multifractality of fine bubbles in turbulence due to lift, Phys. Rev. Fluids **3**, 124305 (2018).

[49] R. Ni and K. Q. Xia, Experimental investigation of pair dispersion with small initial separation in convective turbulent flows, Phys. Rev. E **87**, 063006 (2013).

[50] S. Schwarz, T. Kempe, and J. Fröhlich, A temporal discretization scheme to compute the motion of light particles in viscous flows by an immersed boundary method, J. Comput. Phys. **281**, 591 (2015).

[51] J. Jang and C. Lee, An immersed boundary method for nonuniform grids, J. Comput. Phys. **341**, 1 (2017).

[52] M. Tanaka, Motion of spherical bubbles in homogeneous shear turbulence, Fluid Dynamics Research **51**, 035505 (2019).

Correction: Two rows in Table II were inadvertently duplicated during the production process and have been removed.